JOURNAL OF AIRCRAFT
Vol. 46, No. 1, January–February 2009

Analysis of Solid Oxide Fuel Cell Systems for More-Electric Aircraft

M. Santarelli,* M. Cabrera,† and M. Calì‡
Politecnico di Torino, Torino 10129, Italy

DOI: 10.2514/1.38408

Aviation emissions are growing faster than any other sector and they risk undermining the progress achieved through emission cuts in other areas of the economy. Rapidly emerging hydrogen- and fuel-cell-based technologies could be developed for future replacement of onboard electrical systems in more-electric or all-electric aircraft. The primary advantages of deploying these technologies are low emissions and low noise (important features for commuter airplanes that take off and land in urban areas). Solid oxide fuel-cell systems could be advantageous for some aeronautical applications due to their capability of accepting hydrocarbons and high energy-density fuels. Moreover, they are suitable for operating in combined heat and power configurations; they recover heat from high-temperature exhaust gases, which could be used to supply thermal loads and thereby reduce the electric power requested by the aircraft. Environmentally Friendly Inter City Aircraft Powered by Fuel Cells is a Sixth Framework Programme project selected by the Aeronautics and Space division of the European Commission and led by the Politecnico di Torino in Turin, Italy. One of the objectives of the project is to carry out a feasibility study on different types of more-electric intercity aircraft. After the characterization of the power consumption of electrical and nonelectrical loads, and the definition of mission profiles for three different typologies of passenger aircraft, the design of the solid oxide fuel-cell-based energy system as well as the simulation of complete missions is performed by hypothesizing different system configurations. The simulations concern both the stack (current and current density, cell and stack voltage, etc.) and the balance of plant (air compressor power, gross stack power, system efficiency, etc.). Obtained results are analyzed and discussed.

Nomenclature

E_{rev}	=	open circuit voltage, V
F	=	Faraday number, $\text{C} \cdot \text{mol}^{-1}$
G	=	mass flow, $\text{kg} \cdot \text{s}^{-1}$
h	=	specific enthalpy, $\text{kJ} \cdot \text{kg}^{-1}$
$\bar{h}$	=	molar enthalpy, $\text{kJ} \cdot \text{mol}^{-1}$
I	=	generator current intensity, A
$i_{ç}$	=	current density, $\text{A} \cdot \text{cm}^{-2}$
N	=	molar flow of reactant, $\text{mol} \cdot \text{s}^{-1}$
n_c	=	number of cells
S	=	single cell active area, cm^2
U_f	=	fuel use factor in coded form
U_{ox}	=	air use factor in coded form
V_c	=	single-cell voltage, V
W_{dc}	=	stack electrical power, kW
$W_{\text{el},c}$	=	single-cell electrical power, W
x	=	moles of CH_4 that react, $\text{mol} \cdot \text{s}^{-1}$
y	=	moles of CO that react, $\text{mol} \cdot \text{s}^{-1}$
$\Delta\bar{h}_{\text{react}}$	=	molar enthalpy of chemical reaction, $\text{J} \cdot \text{mol}^{-1}$
$\eta_{\text{act,a/c}}$	=	activation overpotential at anode and cathode, V
$\eta_{\text{conc,a/c}}$	=	concentration overpotential at anode and cathode, V
η_{ohm}	=	ohmic overpotential, V
ϕ_{air}	=	heat for oxidant (air) preheating, kW
ϕ_{diss}	=	heat losses from the complete system, kW
ϕ_{ech}	=	heat of electrochemical reaction, kW
ϕ_{ref}	=	heat of steam reforming reaction, kW
ϕ_{shift}	=	heat of water shift reaction, kW

Received 7 May 2008; revision received 12 July 2008; accepted for publication 16 July 2008.

*Associate Professor, Dipartimento di Energetica, Corso Duca degli Abruzzi 24; massimo.santarelli@polito.it.

†Associate Researcher, Dipartimento di Energetica, Corso Duca degli Abruzzi 24.

‡Full Professor, Dipartimento di Energetica, Corso Duca degli Abruzzi 24.

I. Introduction

AVIATION emissions are growing faster than any other sector, and they risk undermining the progress achieved through emission cuts in other areas of the economy. In the European Union, emissions from international flights grew by 73% from 1990 to 2003. This increase could widen to 150% by 2012. Such growth would cancel out more than a quarter of the 8% reduction in total greenhouse gas emissions that the Kyoto Protocol requires the EU-15 to achieve between 1990 and 2012. Although it accounts for only 4.2% of the total global warming potential, the concern today is that aviation-generated CO_2 is projected to grow to approximately 5.7% by 2050 [1].

The aerospace industry faces pressure from two fronts: the impact of increasing air traffic on the environment, that is, emissions at high altitudes, in atmospheric regions that are characterized by particular dynamics and photochemistry; and the growing public awareness of local air quality around airports, especially near urban areas. This pressure translates to additional constraints on airport capacity (local air quality, mainly) on top of other constraints already in place (e.g., noise restrictions).

Continuous research on new technologies and efficiency improvement of traditional technologies is being performed both by governmental and nongovernmental institutes to reverse the growing trend of pollutant emissions from aviation. Among these new technologies, fuel cells are the object of study of numerous programs around the world.

Rapidly emerging hydrogen- and fuel-cell-based technologies could become an interesting alternative as new propulsion systems for light aircraft and small commuter aircraft. In addition, these technologies can also be developed for the future replacement of onboard electrical systems in larger, more-electric or all-electric aircraft. The primary advantages of deploying these technologies are low emissions and low noise (particularly important features for commuter airplanes, which usually take off and land in urban areas). In particular, the possibility of taking off and landing within the noise abatement regulations set for small airfields in urban areas and near population centers will allow the use of these airfields during late night hours, when the noise abatement regulations are even more stringent. System studies are being conducted to identify concepts

with high payoff potential and associated technology areas for further development.

In the field of aerospace, fuel cells have been used since the 1960s, when NASA began using first proton exchange membrane fuel cells (PEMFC) and then alkaline fuel cells as a primary source of electrical power or as an electrical energy storage device in launch vehicles, Earth-orbiting spacecraft, the space shuttle, crew return vehicles, astronaut equipment, planetary spacecraft, landers, rovers, and penetrators [2]. Recently Boeing has successfully completed the first-ever manned fuel-cell-powered flight. In this 5 year project, a PEMFC, as well as hydrogen storage and supply, were successfully installed in a two-seat lightweight airplane for providing propulsion together with a lithium–ion battery [3].

Solid oxide fuel cells (SOFCs) have not been successfully employed in aeronautics yet, though at least one small SOFC unmanned aerial vehicle (UAV) is reported to have successfully completed several flights (with 60 W of cruise power) [4]. Current research on the use of SOFC systems in aeronautical applications is focused on feasibility studies. Different studies have been carried out by governmental and nongovernmental organizations. A planar, anode-supported cell design stack with a gas turbine bottoming cycle auxiliary power unit (APU) for a 300 passenger commercial transport aircraft was analyzed in [5]. In [6], a suite of component models was developed to estimate the mass, volume, and performance for a given system architecture. These models include a hydrogen–air polymer electrolyte membrane (PEM) fuel cell, SOFC, balance-of-plant components (compressor, humidifier, separator, and heat exchangers), compressed gas, cryogenic and liquid fuel storage tanks, and gas turbine/generator models for hybrid system applications. Parametric mass and volume models for a hybrid SOFC/gas turbine APU were developed in [7], linking the thermodynamic model to the mass and volume model and providing immediate feedback during the design process. The feasibility of replacing traditional APUs with SOFC generators was treated in [8].

In [9], the functionality and evaluation of the propulsion and power system benefits derived from a SOFC-based APU for a future long-range commercial aircraft were defined, and the technology gaps to enable such a system were analyzed. The study employed technologies commensurate with entry into service in 2015.

SOFC and PEM fuel cells are the most developed and employed types of fuel-cell technologies for mobile applications. PEM fuel cells present some advantages, such as faster startups and load following and the highest power density compared with other fuel cells (FC) (up to 1.2 kW/kg), and, because they are committed to operating with very pure hydrogen, no pollutant emissions to the atmosphere are generated. However, some drawbacks could limit the use of these fuel cells in aeronautical applications. In the first place, a nonhomogeneous distribution of the water inside the membrane due to inertial forces could affect the stability of the generator. In addition, low temperatures at high altitudes may increase the risk of water freezing inside the stack. Besides, a more complex balance of plant (water management, stack cooling system, etc.) may represent larger and heavier systems to be placed inside the aircraft. In aeronautics, probably the biggest limitation of PEM fuel cells is that they operate only on pure hydrogen. Even though on an equal mass basis the energy content of hydrogen is by far higher than all hydrocarbon fuels, meaning that the term "kilograms of fuel per mission" is significantly reduced if running on hydrogen, the extremely low density of hydrogen implies carrying on the aircraft huge storage systems for current storage pressures (up to 700 bar) or cryogenic tanks, which are lighter and more compact than a high-pressure gaseous storage tank for the same mass of hydrogen but still larger than the storage systems for commonly used hydrocarbon fuels. Another alternative is including a fuel-processing system or other procedures (photolysis, reforming, electrolysis) for producing hydrogen onboard, which adds mass and complexity to the overall system.

On the other hand, even if they present long startup times and slow stabilization due to high thermal inertia, as well as lower power densities compared with PEMFC, SOFC systems could be advantageous for some aeronautical applications due to their capability of accepting hydrocarbons and high energy-density fuels. Theoretically, once gasified, SOFC generators could even operate on liquid fuels such as jet fuel [10], and so most of the already applied fuel storage and distribution system would remain the same. Besides, with no need of water management or an external cooling system, the balance of system in the case of SOFC is simpler. Moreover, SOFCs have low sensitivity to high inertial forces due to the solid electrolyte. A significant feature of SOFCs is that they are suitable for operating in combined heat and power (CHP) configurations, recovering heat from the high-temperature exhaust gases; the heat recovered at high temperatures could be used to supply different loads, especially thermal loads, thereby reducing the electric power requested by the aircraft and consequently allowing a size reduction of the primary generator.

It is important to remark that the only nonpollutant solution is that of using pure hydrogen for feeding the stack. When running on hydrocarbons, SOFC systems deliver pollutant emissions into the atmosphere. Nevertheless, these emissions are reduced when compared with traditional heat engines due to the improved efficiencies of SOFC systems. Of course, SOFCs could also be fed on pure hydrogen but, in such a case, the same fuel storage problems that affect PEM fuel cells would affect the SOFC system as well. In [11], a SOFC/gas turbine system fed with liquid hydrogen to provide primary or secondary electrical power for a UAV over a high-altitude, long-endurance mission is described.

In this work, after the definition and characterization of the power consumption of the electrical and nonelectrical loads of three different kinds of transport aircraft [regional jet (RJ), small commuter (SC), and air taxi (AT)] and the definition of a mission profile, the design of the SOFC-based energy system as well as the simulation of a complete mission for each aircraft typology was performed considering different system configurations. The obtained results are discussed.

II. Environmentally Friendly Inter City Aircraft Powered by Fuel Cells Project

The Environmentally Friendly Inter City Aircraft powered by Fuel Cells (ENFICA-FC) project (contract no. 030779—AST5-CT-2006-030779), led by Politecnico di Torino in Turin, Italy, and made up of 10 partners, has been selected by the Aeronautics and Space division of the European Commission as the Sixth Framework Programme (FP6). The project involves key intercity aircraft as well as leading fuel-cell experts with an overall budget of 4.5 million euros, of which 2.9 million euros will be funded by the European Commission. Through this project, the associated research and industrial consortium partners aim to develop and provide operational zero-pollution solutions to the immediate needs of aircraft services.

Its main goal is to study and demonstrate the possibility of obtaining a more-/all-electric aircraft through the integration of fuel-cell technology as the main power-supply system. During the 3-year research activity, a fuel-cell-based power system will be designed, developed, and installed in an ultralight aircraft to achieve the first fuel-cell-manned flight.

Another objective of the ENFICA-FC project is to carry out a feasibility study on different categories of more-electric intercity aircraft, providing a preliminary definition of new forms of aircraft systems that can be supplied by fuel-cell technologies (auxiliary power unit, primary electrical generation supply, emergency electrical power supply, landing gear, de-icing system, etc.). In particular, three aircraft types have been taken into consideration: air taxi (5 seats), small commuter (9 seats), and regional jet (32 seats).

A good example of a small regional jet is the Dornier 328JET (see Fig. 1). It is a regional airliner with 32 passengers at 79 cm (31 in.) seat pitch with the following engineering designations: 328-300 and 328-310 [12]. With regard to a small commuter and an air taxi, good examples of these types of aircraft are Evektor's VUT 100-120i Cobra and EV-55 Outback, respectively. Specifications of the three analyzed aircraft are shown in Table 1.

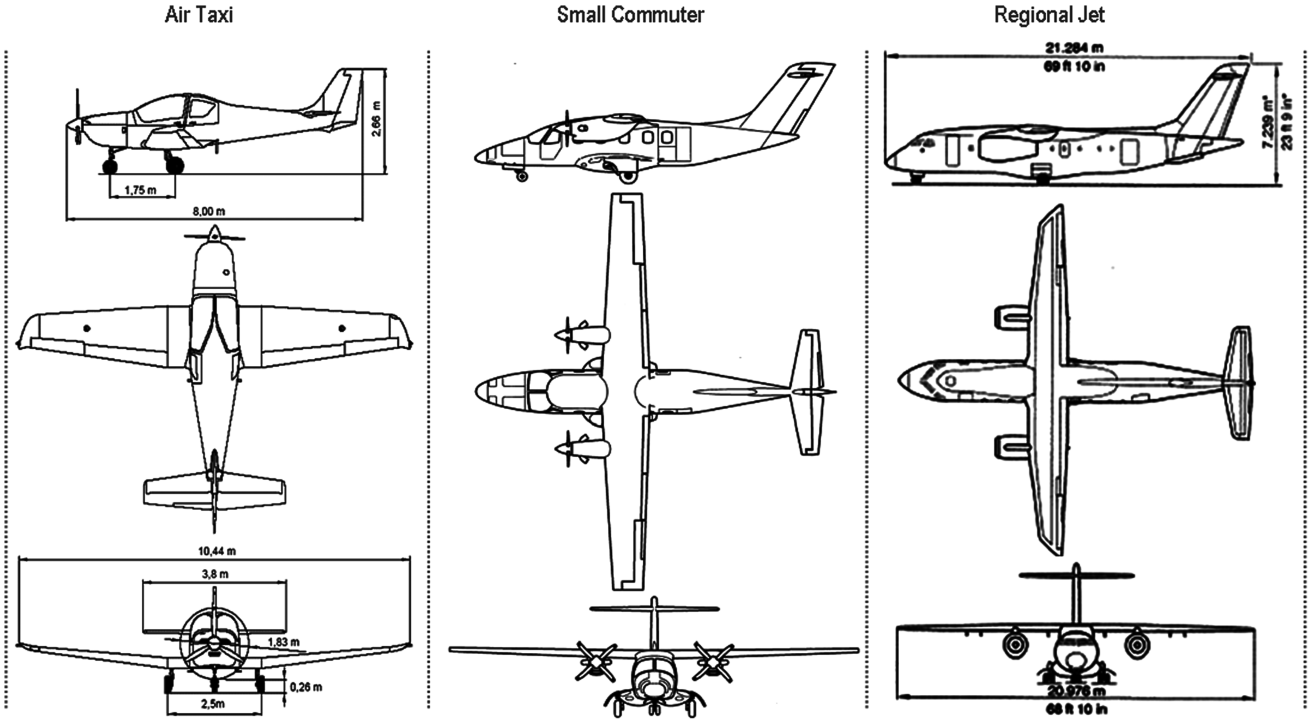

Fig. 1 Three views of the air taxi, small commuter, and regional jet.

Because of its capability of being fed by various high-density fuels (e.g., jet fuels), high efficiency, and heat recovery capability, a SOFC-based system could efficiently suit the needs of the onboard systems of more-electric air taxis, small commuters, and regional jets.

III. Typical Mission Profiles: Considerations About Solid Oxide Fuel-Cell Use

After identifying the electrical systems to be supplied by the SOFC generator, a typical mission has been hypothesized and described in terms of range profile and load profile, depending on the capacities and requirements of each aircraft category. The range profile of each analyzed mission can be seen in Fig. 2. The entire flight has been divided into representative phases, from preparation on the ground to taxiing in, and each single-system electrical load has been defined, making it possible to determine the load profiles during the mission. With regard to the air taxi and small commuter, a simple take-off-climb-cruise-descent-landing mission has been hypothesized. For the regional jet, the possibility of bad weather conditions or other events that could force the aircraft to a second climb out to a second airport after already approaching the destination airport have been taken into account, so that an alternate descent, a 10 min hold phase at 1500 m, and an alternate climb have been considered.

As a matter of example, the load profile of a typical mission for a more-electric regional jet is shown in Table 2 [12], in which the electrical loads of the onboard systems (that should be supplied by the generator) in the different phases of the flight are described. In a preliminary approach, the maximum electrical load is 82.4 kW during the phase of takeoff and climb.

The consumptions described in Table 2 correspond, nevertheless, to a more-electric configuration in which all the onboard systems are supplied electrically by the fuel-cell APU. When using a SOFC generator, some of the loads of a more-electric aircraft, which are supposed to be covered with electricity, can be treated in fact as thermal loads (just like it is done currently with the traditional heat engines), because SOFC systems are ideal for operating in a CHP configuration with the temperature of the exhaust gases from around 250 up to 300°C. This is an advantage over other kinds of fuel cells, such as in PEM systems, in which the waste heat is not very useful because it is available only at low temperatures (nearly 60°C).

If some loads are supplied directly with the recovered thermal power, the total electric load to be covered by the fuel-cell generator is reduced. Reducing the maximum electric power that should be provided by the SOFC system also reduces its size and mass, which are critical aspects when it comes to aeronautical applications.

The feasibility of converting some of the electric loads directly as thermal loads has been studied in the regional jet, including in particular the air conditioning heating (ACH), the ice and rain

Table 1 Specifications for the Dornier 328Jet, the Evektor VUT 100-120i Cobra, and the EV-55 Outback

		Air taxi	Small commuter	Regional jet
Capacity		5 seats	9 seats	32 seats (up to 34)
Power plant		1x Textron Lycoming IO-360 4-cylinder, 200 hp (149 kW)	2x Pratt and Whitney Canada PT6A-21 max takeoff power 536 shp 400 kW	2x Pratt and Whitney Canada PW 306B
Propeller		MTV-12/B183-59d3 blade, constant speed diameter 183 cm	AVIA AV 8444 blade, constant speed diameter 2,082 m	——
Weights	Max. takeoff, kg	1330	4600	15,200
	Max. payload, kg	500	1824	3410
Performance	Max. operating speed, km/h	287	380	——
	Stall speed, km/h	93	142.7	——
	Range, km	2000	2258	——

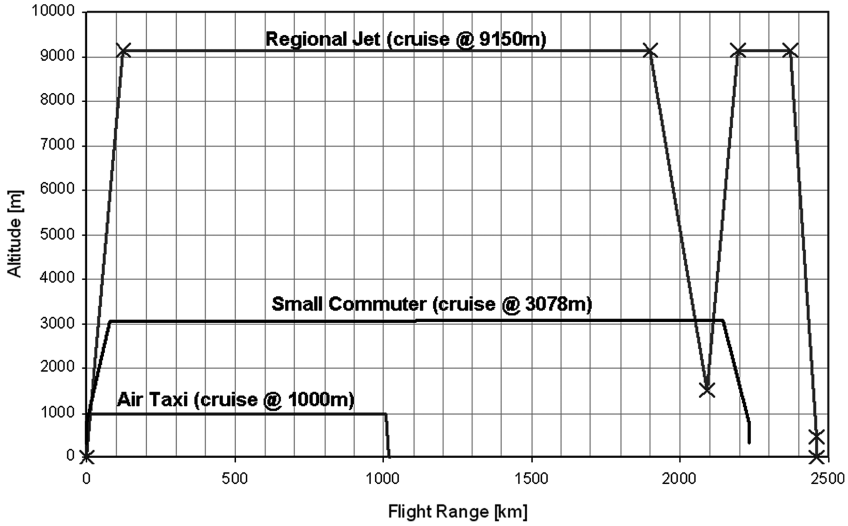

Fig. 2 Typical mission range profile for the three aircraft typologies.

protection system, and the heating (baggage compartment and windshield).

Supplying the regional jet's ice and rain protection system with recovered heat from the SOFC system is unpractical because this would require a high amount of heat, and only a small fraction could be provided even when generating the maximum electric power. The more practical use for the recovered heat from the SOFC system results in covering the thermal load of the ACH.

To make the evaluations, real data on thermal recovery from a real, operating SOFC system managed by the authors [13] have been taken into account.

Because of conversion efficiencies of the heat recovery system (heat exchanger, pipes, etc.), the gross thermal power required upstream of the heat recovery system would differ from the electrical power required to cover the same loads in the form of electrical loads. In the case of the preliminary analysis, a conservative 80% heat exchange system efficiency has been considered.

Reducing the gross electric power output also reduces the heat that could be recovered from the exhaust gases. Because it has been hypothesized that the generator must follow the load profile during the mission, in some phases (at a low electrical load) the thermal power recovered is not enough to cover the thermal load. A reasonable solution could be an integrated system in which the remaining thermal load is supplied directly with an electric power surplus. As shown in Fig. 3, the gas-to-gas heat exchangers (5) are introduced upstream of the electric heaters (4). Thus, the heat contained in the exhaust gas from the SOFC generator is recovered in every phase of the mission and fed to the ACH. The integration of electric and thermal power for supplying the ACH takes place only at low electrical loads; at high electrical loads, the recoverable heat is enough to provide the entire thermal load.

The whole mission profile is then modified according to the modified electrical load presented in Table 3 (considering, as an example, just the regional jet), bypassing thermal power or integrating thermal and electric power depending on the ACH load required in each mission phase.

The ACH electric load is no longer considered, but it is set as the thermal load. Two more rows have been added. One shows the recoverable heat from the exhaust gas, taking into consideration the efficiency of the heat exchange system; it represents the effective thermal power downstream of the heat exchangers. As already established, if the effective recoverable heat is lower than the thermal load, an electric power surplus is needed for supplying the rest of the load.

Recall that an electric power surplus implies an increase in the recoverable thermal power; therefore, the electric power surplus will not simply coincide with the first-iteration difference between the thermal load and the effective thermal power, but it will be lower because of the increase of the relative recoverable heat. This variation has been considered while constructing the preliminary power profiles, such as the one presented in Table 3.

The maximum electric power to be provided by the SOFC generator is then reduced. In the case of the regional jet, during the high-load phases, no electric power surplus is needed, and so the new electrical load is simply found by subtracting the ACH load (20 kW) from the original electrical load. The maximum net electrical power is reduced from 82.4 to 62.4 kW. The nominal power is reduced and so is the size and mass of the generator.

Table 2 Regional jet single-system electrical load (all loads in kW)

	APU on gnd	Start	Taxi out	Takeoff & climb	Cruise	Descent	Hold	Climb altern.	Cruise altern.	Descent altern.	Aprch & landing	Taxi in
Engine starting	——	28	——	——	——	——	——	——	——	——	——	——
Air cond.	8	——	8	15	25	15	10	15	25	15	8	8
AC heating	20	0	20	20	20	20	20	20	20	20	20	20
Ice & rain protection	——	——	——	30	——	30	30	30	——	30	——	——
Heating	1.0	——	6.5	6.5	6.5	6.5	6.5	6.5	6.5	6.5	6.5	6.5
El. pwr. sys.	0.6	0.6	0.4	0.3	0.2	0.2	0.2	0.3	0.2	0.2	0.2	0.4
Systems	1.2	1.2	0.1	0.1	0.2	0.1	0.1	0.1	0.2	0.1	0.1	0.1
Avionics	3.7	3.7	3.7	3.7	3.7	3.7	3.7	3.7	3.7	3.7	3.7	3.7
Lights	0.8	0.3	1.5	1.0	1.0	1.0	1.0	1.0	1.0	1.0	1.3	1.5
Flight control	5.8	5.8	7.1	5.8	5.8	5.8	5.8	5.8	5.8	5.8	5.8	9.5
Total power, kW	*41.1*	*39.6*	*47.3*	*82.4*	*62.4*	*82.3*	*77.3*	*82.4*	*62.4*	*82.3*	*45.6*	*49.7*
Time, min	15.2	1.0	20.0	12	178.0	21.0	10.0	10.0	17.5	10.0	3.3	8.0
Range, km	0.0	0.0	0.0	122.0	1778	190.0	0.0	105.0	175.0	90.0	0.0	0.0

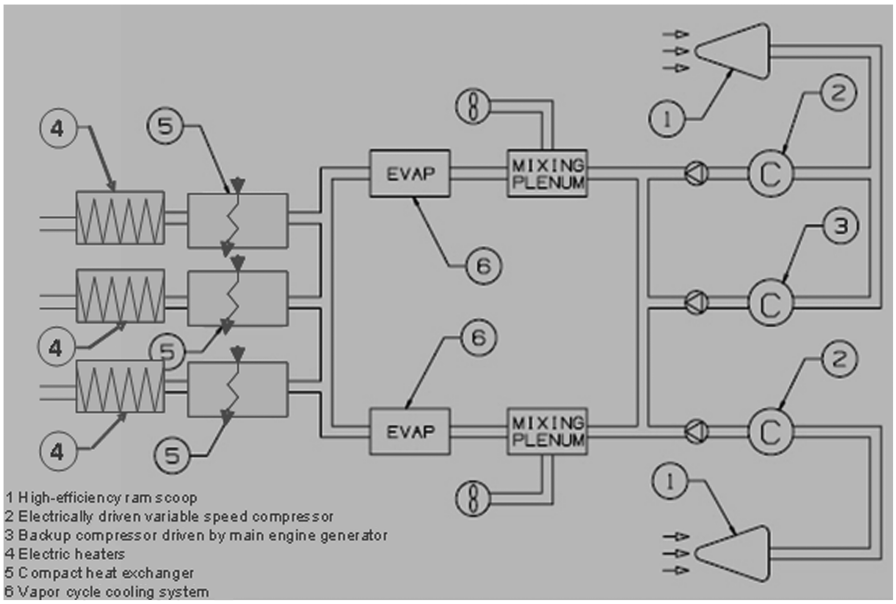

Fig. 3 Integrated environment control system.

The same hypotheses have been applied to the small commuter. The main difference is that, when treating the ACH system as a thermal load, the whole electrical load of the rest of the systems is lower than the ACH thermal load in all mission phases except for the start phase, during which this system is, however, turned off. Thus, the power supply for ACH is mostly electric, and thermal integration only helps to reduce the electrical load of this system. The size of the stack is not affected in this case because the maximum electrical load (16.7 kW, start phase) does not change. Heat recovery is therefore useful in the reduction of the electric loads and, consequently, of the fuel consumption.

With regard to the air taxi, the heating system load is also too high to be provided only with recovered heat from the fuel-cell system, and so electric power should be supplied during the entire mission. Because heating is currently supplied with thermal power recovered from the exhaust of the internal combustion engine that provides propulsion, and the energy contained in these gases would be otherwise released into the atmosphere, the decision has been made to not cover the heating system load with power from the fuel-cell generator but to leave it unchanged. Supplying heating in this kind of aircraft with both electrical or thermal power from a SOFC generator does not result in fuel savings or efficiency of the main engine improvement. On the contrary, it only increases the fuel consumption of the stack and, with it, the overall fuel consumption. This is not the case of the small commuter aircraft, in which the energy source for the ACH is compressed air extracted from the turboprop engines, affecting their efficiency and, therefore, the fuel consumption of the aircraft.

The original and modified abbreviated load profiles of the typical missions of the small commuter and air taxi are presented in Tables 4 and 5 and in Table 6, respectively. The maximum electrical load of the small commuter is not reduced. However, the electrical load does decrease in most phases of the mission due to the heat recovery solution proposed, reducing the overall fuel consumption. Also, in the load profile of the air taxi, the maximum electrical load remains constant (4.6 kW), corresponding to the start phase in which the ACH does not work. On the other hand, in almost every other phase of the flight, the electrical load is significantly reduced (thanks to the exhausts of the internal combustion engine that provides propulsion), as is the fuel consumption of the stack and, with it, the size and mass of the fuel tank.

IV. Model of Solid Oxide Fuel-Cell Plant Fed with Natural Gas

Two SOFC technologies have been analyzed, based on the geometry of the single cell: a tubular-cell configuration (TC) stack and a planar-cell configuration (PC) stack. The fuel considered is the

Table 3 Regional jet modified load profile with heat recovery from SOFC (all loads in kW)

	APU on gnd	Start	Taxi out	Takeoff & climb	Cruise	Descent	Hold	Climb altern.	Cruise altern.	Descent altern.	Aprch & landing	Taxi in
Engine starting	——	28	——	——	——	——	——	——	——	——	——	——
Air Cond.	8		8	15	25	15	10	15	25	15	8	8
AC heating	0	0	0	0	0	0	0	0	0	0	0	0
Ice & rain protection	——	——	——	30	——	30	30	30		30	——	——
Heating	1.0	——	6.5	6.5	6.5	6.5	6.5	6.5	6.5	6.5	6.5	6.5
El. pwr. sys.	0.6	0.6	0.4	0.3	0.2	0.2	0.2	0.3	0.2	0.2	0.2	0.4
Systems	1.2	1.2	0.1	0.1	0.2	0.1	0.1	0.1	0.2	0.1	0.1	0.1
Avionics	3.7	3.7	3.7	3.7	3.7	3.7	3.7	3.7	3.7	3.7	3.7	3.7
Lights	0.8	0.3	1.5	1.0	1.0	1.0	1.0	1.0	1.0	1.0	1.3	1.5
Flight Control	5.8	5.8	7.1	5.8	5.8	5.8	5.8	5.8	5.8	5.8	5.8	9.5
Thermal load	20	0	20	20	20	20	20	20	20	20	20	20
El. pwr. (mod.), kW	*29.3*	*39.6*	*33.8*	*62.4*	*44.6*	*62.3*	*57.3*	*62.4*	*44.6*	*62.3*	*32.6*	*35.5*
El. pwr. surplus, kW	8.3	0.0	6.5	0.0	2.2	0.0	0.0	0.0	2.2	0.0	7.0	5.8
Recoverable heat (eff.), kW	11.7	0.0	6.5	0.0	2.2	0.0	0.0	0.0	2.2	0.0	7.0	5.8
Time, min	15.2	1.0	20.0	12	178.0	21.0	10.0	10.0	17.5	10.0	3.3	8.0
Range, km	0.0	0.0	0.0	122.0	1778	190.0	0.0	105.0	175.0	90.0	0.0	0.0

Table 4 Original small commuter load profile

	Preparation	Start	Taxi out	Takeoff	Climb	Cruise	Descent	Landing	Taxi in
Electric power, no ACH; W	761.6	16,728.9	6533.3	4733.0	3340.1	3918.9	4460.1	5453.7	6890.3
Electric power to ACH, W	——	——	9228.0	9228.0	——	9228.0	——	9228.0	9228.0
Total electric power, W	*761.6*	*16,728.9*	*15,761.3*	*13,961.1*	*3340.12*	*13,146.9*	*4460.1*	*14,681.7*	*16,118.3*
Time, min	5	0.3	4	0.47	12.71	310.89	12.71	2.5	4
Range, km	0	0	1	0	78.5	2067	88.4	0	1

Table 5 Modified small commuter load profile

	Preparation	Start	Taxi out	Takeoff	Climb	Cruise	Descent	Landing	Taxi in
Electric power, no ACH; W	761.6	16,728.9	6533.3	4733.0	3340.1	3918.9	4460.1	5453.7	6890.3
Total ACH load, W			9228.0	9228.0		9228.0		9228.0	9228.0
Recoverable heat, W	304.6	6691.6	4503.2	3988.9	1336.0	3756.3	1784.0	4194.8	4605.2
Electric power surplus, W	0	0	4724.8	5239.1	0	5471.7	0	5033.2	4622.8
Total electric power, W	*761.6*	*16,728.9*	*11,258.1*	*9972.2*	*3340.1*	*9390.6*	*4460.1*	*10,486.9*	*11,513.1*
Time, min	5	0.3	4	0.47	12.71	310.89	12.71	2.5	4
Range, km	0	0	1	0	78.5	2067	88.4	0	1

Table 6 Load profile with and without heating (air taxi)

	Preparation	Start	Taxi out	Takeoff	Climb	Cruise	Descent	Landing	Taxi in
Electric power with heating, W	146.5	4602.3	2717.7	3038.3	3038.3	2898.6	3271.0	3271.0	2503.6
Total heating load, W			1263.3	1263.3	1263.3	1263.3	1263.3	1263.3	1263.3
Electric power, no heating; W	*146.5*	*4602.3*	*1454.4*	*1775.0*	*1775.0*	*1635.3*	*2007.7*	*2007.7*	*1240.3*
Time, min	5	0.2	2	1	3.6	240	4.5	2.5	2
Range, km	0	0	0.5	0.5	8.7	1000	11.31	0.44	0.5

most used in SOFC: natural gas. Both stacks are integrated with a catalytic prereformer for the natural gas fuel and a combustor where the postcombustion of the depleted fuel and the air exiting the cell occurs. The whole system is integrated with other auxiliaries (heat exchangers, blowers, valves, etc.) and is defined as balance of plant (BOP). Before entering the BOP, the fuel flow is desulphurized; inside the BOP, it is sent to the ejectors in the stack. In fact, part of the anode exhaust gas is recirculated in the fuel stream to supply water for the fuel internal reforming reaction. With present technology conditions, and because of the different geometries (causing different electron paths in the cells), to get sufficient performance the TC has to operate at a higher temperature (around 970°C), whereas the PC is allowed to operate at a reduced temperature (around 800°C) with similar performance. In both cases, because the generator operates at a high temperature, a heat flow from the stack exhausts can be recovered at the outlet of the plant. Exhaust gases leave the generator skid at about 850–900°C for TC and about 770°C in the case of PC. Subsequently, in the thermal management system, the exhausts exchange heat with the incoming process air in a heat recovery system [13].

The rest of the BOP is composed by six major skids: generator module, electrical control system, fuel supply system, air compressor, thermal management system, and heat export system. A simplified flow diagram of the BOP of the SOFC system is shown in Fig. 4.

Modeling an SOFC stack involves the electrochemical and the chemical model, as well as the BOP model [14]. The electrochemical model refers to the polarization curve; overpotentials are modeled considering their dependence on the average generator temperature.

A generalized expression of the polarization curve for a solid oxide fuel cell is

$$V_c = E_{\text{rev}} - \eta_{\text{act,a/c}} - \eta_{\text{ohm}} - \eta_{\text{conc,a/c}} \tag{1}$$

where V_c is the single-cell voltage, E_{rev} is the reversible (open circuit) voltage, $\eta_{\text{act,a/c}}$ is the activation overpotential, η_{ohm} is the ohmic overpotential, and $\eta_{\text{conc,a/c}}$ is the concentration overpotential. Equations suggested in [13–18] have been considered for describing the polarization of both geometrical configurations of the SOFC. Some works have been taken into account in setting some specific

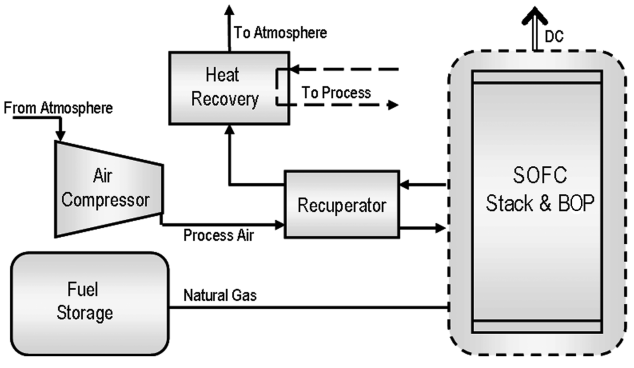

Fig. 4 Example of an SOFC system layout.

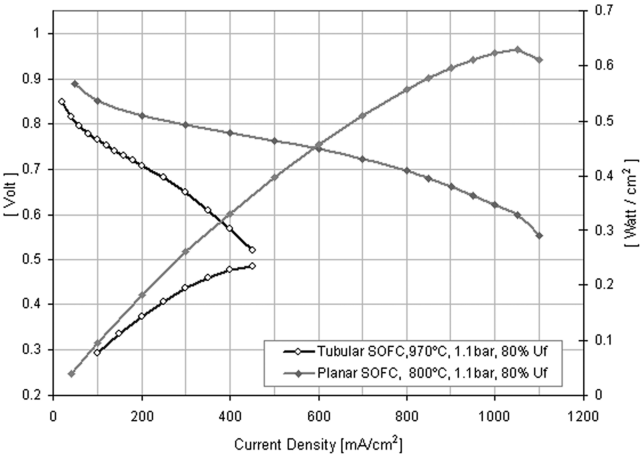

Fig. 5 Polarization of the different typologies of SOFC.

Table 7 Equations used in the balance-of-plant model

Heat of steam reforming reaction	$\phi_{\text{ref}} = x(3h_{\text{H}_2} + h_{\text{CO}} - h_{\text{H}_2\text{O}} - h_{\text{CH}_4})$	(4)
Heat of water shift reaction	$\phi_{\text{shift}} = y(\bar{h}_{\text{H}_2} + \bar{h}_{\text{CO}} - \bar{h}_{\text{H}_2\text{O}} - \bar{h}_{\text{CH}_4})$	(5)
Heat of electrochemical reaction	$\phi_{\text{ech}} = n_c I\left(\frac{-\Delta\bar{h}(T_{\text{gen}})}{2F} - V_C\right)$	(6)
Single-cell electrical power	$W_{\text{el},c} = i_c S V_C$	(7)
Oxidant preheating	$\phi_{\text{air}} = G_{\text{air}}\Delta h_{\text{air}}$	(8)
Heat recovered from the exhausts	$\phi_{\text{exh}} = G_{\text{exh}}\Delta h_{\text{exh}}$	(9)
Generator thermal balance:	$W_{\text{dc}} = \sum_{\text{ch}_{\text{in}}=1}^{N_{\text{in}}} G_{\text{ch}_{\text{in}}} h_{\text{ch}_{\text{in}}} - \sum_{\text{ch}_{\text{out}}=1}^{N_{\text{out}}} G_{\text{ch}_{\text{out}}} h_{\text{ch}_{\text{out}}} + \sum_{\text{ch}_{\text{react}}=1}^{N_{\text{react}}} \dot{N}_{\text{react}}(-\Delta\bar{h}_{\text{react}}) - \phi_{\text{diss}}$	(10)

parameters, such as porosity and tortuosity [19,20]. Fundamental binary diffusivities of reactant mixtures are evaluated according to the Chapman–Enskog model [21,22].

Examples of tubular and planar cell polarization curves are presented in Fig. 5. As can be observed in the figure, the polarization performance of planar cells is better. This means that, when operating at the same current density, the voltage of a planar-geometry cell is higher than that of a tubular cell. In addition, tubular cells operate within a limited range of current density and, for these cells, a common operation point would be 200 mA/cm^2; for planar cells, it would be up to 900 mA/cm^2.

With better polarization performance, planar cells offer higher power densities (see Fig. 5). Thus, at a given current density of operation, the same power output would require less active surface, reducing the size of the stack. From the power density curves, fixing the single cell active surface, a preliminary number of cells needed for supplying a given load can be easily established.

The reason for the better performance of planar cells, or rather, the reason for the low performance of tubular cells, is essentially the high ohmic drop due to the long paths of the electrons in the tubular electrodes while moving from one cell to another. These electronic paths depend on the way in which the cells are connected to each other and, thus, on the position of the interconnect.

Ohmic losses are linked to the composition of the different cell layers or, more specifically, to their resistivity. Ohmic resistance is modeled considering the materials of the layers (electrolyte, electrodes) and any contact resistance between interfaces and between current collectors. Cathode resistivity, in particular, has been estimated by considering this element as composed of two different layers: the current collector layer and the functional layer [17]. The considered TC has the following composition: a 2.2 mm lanthanum strontium manganite oxide (LSM) cathode support, a 40 μm yttria-stabilized-zirconia (YSZ) electrolyte, and a 100 μm cermet Ni + YSZ anode. Planar cells, on the other hand, are composed of the following: a 500–520 μm NiO/8YSZ anode support, a 4–6 μm 8YSZ electrolyte, a 14–16 μm LSM/8YSZ cathode active layer, and a 18–20 μm pure LSM current collector layer.

The chemical model of the SOFC system considers the fuel processing reactions (steam reforming, water shift) taking place inside the stack, where the reactions are considered to be in equilibrium at the reactor temperature. The equilibrium constant of the chemical reactions has been estimated as suggested in [15]:

$$\text{steam reforming}: \text{CH}_4 + \text{H}_2\text{O} \leftrightarrow 3\text{H}_2 + \text{CO} \tag{2}$$

$$\text{water shift}: \text{CO} + \text{H}_2\text{O} \leftrightarrow \text{H}_2 + \text{CO}_2 \tag{3}$$

Finally, the BOP model integrates the stack model with a thermal model (taking into account the energy balance equations of the thermal processes taking place inside the generator) and the chemical species mass balance. It also accounts for devices that define the SOFC plant, such as the air compressor and the heat exchangers for preheating the inlet gases or exporting heat from the exhaust gas. The BOP model does not change from one geometrical configuration of a SOFC single cell to another. Equations used in the BOP model are shown in Table 7.

Stack and auxiliary devices are modeled using a zero-dimensional approach. Steady-state conditions are assumed. Using a computer-based model of a complete SOFC stack and BOP, the main operation variables of the system during each phase of the typical mission, as well as the fuel consumption, have been calculated. The nominal power of the system, and therefore the stack sizing (number of cells,

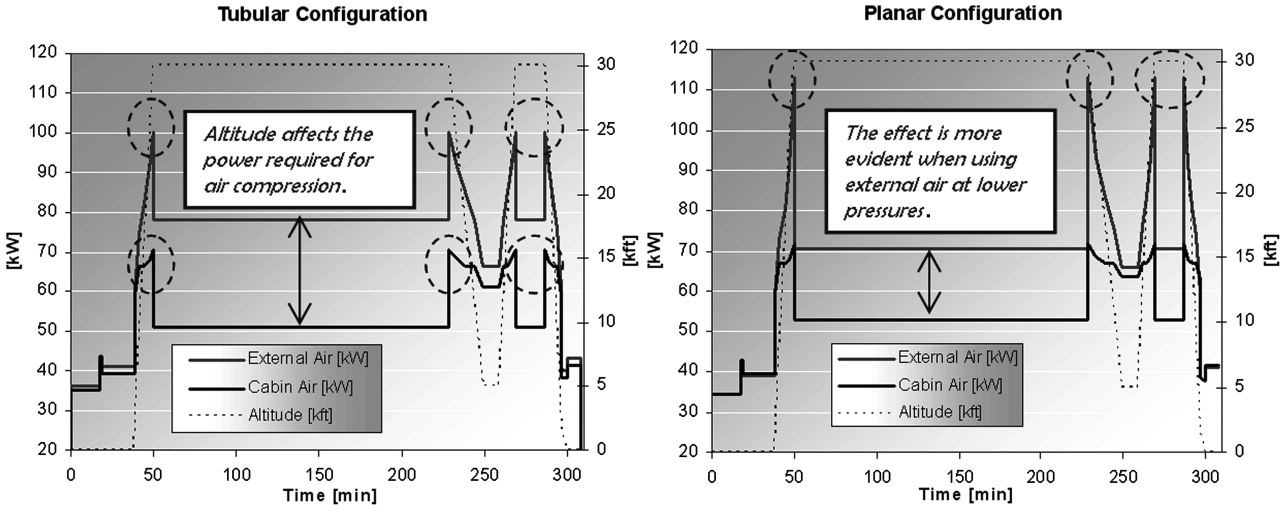

Fig. 6 Gross electric power during the mission (RJ).

Table 8 Stack sizing

			Gross electric power, kW	Number of cells	Number of cells in parallel	Number of cells in series	Single-cell surface, cm^2	Stack volume, l	Stack mass, kg
Air taxi		TC	4.80	39	3	13	834	57.12	32.90
		PC	4.78	38	2	19	250	2.83	18.99
Small comm.		TC	18.1	156	3	52	834	228.50	131.58
		PC	17.7	134	2	67	250	8.29	53.81
Reg. jet	TC	Ext. air	102	960	3	320	834	1406.00	809.74
		Cabin air	77	720	3	240	834	1054.00	607.30
	PC	Ext. air	114	764	2	382	250	44.75	287.46
		Cabin air	72	498	2	249	250	29.65	191.01

BOP), have been estimated on the basis of the maximum gross electrical load during the mission, also taking into account the power consumed by the air compressor in the worst-case scenario. The effect of altitude over the stack has been taken into account in terms of the thermodynamic conditions of the intake air.

The inputs of the model are as follows: the electric load profile (operating current density), the thermal load profile, and the altitude profile (pressure and temperature at air compressor inlet). The outputs of the model are as follows: the electric power (gross, net), the recoverable heat, the fuel consumption, the efficiency (electrical, thermal, overall), and the air mass flow (air compressor consumption).

V. Mission Simulations

The study was performed for two different geometrical configurations of SOFC: tubular SOFC (TC) and planar SOFC (PC).

The first configuration corresponds to a fuel-cell typology developed by Siemens power generation stationary fuel cells with an active surface of 834 cm^2 and a characteristic operating current density of 200 mA/cm^2. The main advantage of tubular cells is the seal-less configuration, which prevents gas leakage and the mixing of reactants. On the other hand, the power density of this configuration is very low (close to 0.1 W/cm^2), resulting in big and heavy stacks that may not be the optimal choice for aeronautical applications.

The PC configuration corresponds to an anode-supported planar cell with an active surface of 150 cm^2 and a characteristic operating current density of 900 mA/cm^2. Even though sealing could be an issue, planar-cell stacks are much more compact than TC stacks due to higher power densities (in the configuration concerning this work, close to 0.8 W/cm^2).

Only in the case of the regional jet, with a high-altitude cruise phase, have two hypotheses regarding two different system configurations been analyzed for each type of cell: case 1 and case 2.

In case 1, the SOFC system is fed with natural gas and external air, which is compressed up to the operating pressure of the stack. The system efficiency is highly affected by the low external air pressure during the mission, which is the intake pressure of the air compressor

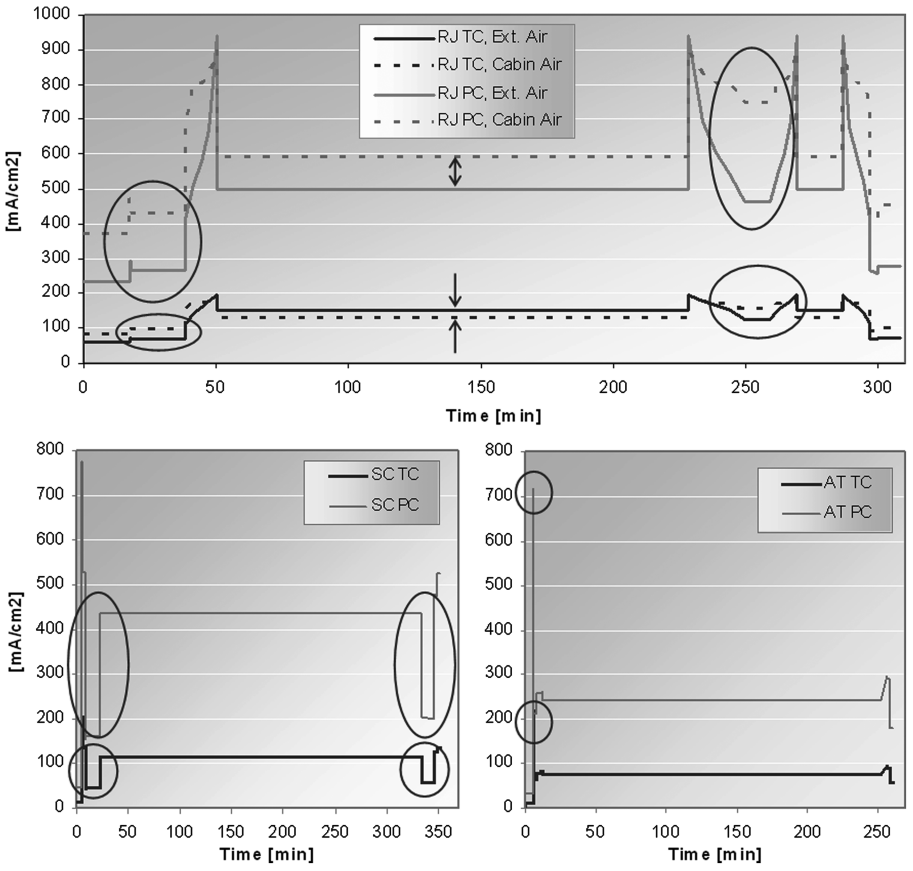

Fig. 7 Current density during the mission.

(see Fig. 6). Work spent on air compression also affects the gross electric power output of the stack and, therefore, the size of the stack and of its BOP.

In case 2, the generator is fed with natural gas and air from the passenger cabin that is compressed to the operating pressure of the stack. With a fixed maximum pressure differential between the passenger cabin and the external air, the air compressor intake pressure (that coincides with the cabin pressure) is kept high during the entire mission; consequently, the compression power is reduced and so is the gross electric power output of the stack. The stack size and mass are significantly reduced, as well as the reactant flow rates; thus, the size and mass of the BOP is also reduced. When modeling the system in case 2, the air composition variation due to passengers breathing has been taken into account, which was shown to be not significant because the concentration of oxygen in the feed air decreases less than 0.02%.

With regard to the small commuter, only the use of external air has been considered; the impact of the external ambient pressure is limited because of the relatively low altitude reached during the flight. Because the air taxi flies at a low altitude (about 1000 m), its cabin is not pressurized.

With lower operation temperatures, a higher rate of feed air is required for cooling down the PC stack. In fact, air use (U_{ox}), which is the number of parts of feed air required for chemical reactions for every 100 parts of air sent into the stack, is equal to 25% in the case of TC and is then reduced to about 20% when hypothesizing the use of planar cells. With regard to the fuel use factor (U_f), it has been kept constant at 80% for both geometrical configurations to compare the behavior and fuel consumption of the stacks with the same boundary condition.

At high loads, when higher rates of stoichiometric air are required, the impact of a lower air-use factor in terms of kilowatts spent for air compression is even more evident. This phenomenon can be observed in Fig. 6, in which the power peaks of the PC stack are higher than those of the TC stack for the regional jet's typical mission. The nominal power of the stack is then higher in the case of PC (see Table 8).

The better performance of planar cells (cell voltage) makes it possible to obtain the same power output at a lower current intensity and, therefore, a lower the rate of stoichiometric air. The current during the mission is equal to the operating current density multiplied by the total active surface, which is 2502 cm^2 (three in-parallel cells of 834 cm^2) for TC and 500 cm^2 (two 250 cm^2 cells) for PC (see Table 8). Even if the operating current density of the PC stack is higher than that of TC during the entire mission, as can be seen in Fig. 7, the current intensity as well as the stoichiometric air request are lower at some points.

Also in Fig. 6, during the cruise phase, the load drop when using cabin air implies an operating current density drop (see Fig. 7). In the case of PC, even though air use is lower, higher cell voltage allows a lower operating current intensity, which means less stoichiometric air. The required stoichiometric air difference in this phase outdoes the 5% air use difference between both configurations, and so the mass rate of feed air is higher for TC, increasing the air compressor load and, consequently, the gross electric power output of the stack. This also explains the reduced size of PC compared with TC in the case of cabin air. The fuel consumption of the PC stack of the regional jet is also reduced during the cruise phase due to lower operating current intensity (see Fig. 12).

Results obtained regarding stack sizing are presented in Table 8. The number of cells in parallel has been chosen on the basis of a current that has been kept below 500 A. In the table, the gross electric power of the stack is also shown, which takes into account the electric power supplied to the air compressor. The mass and volume of the

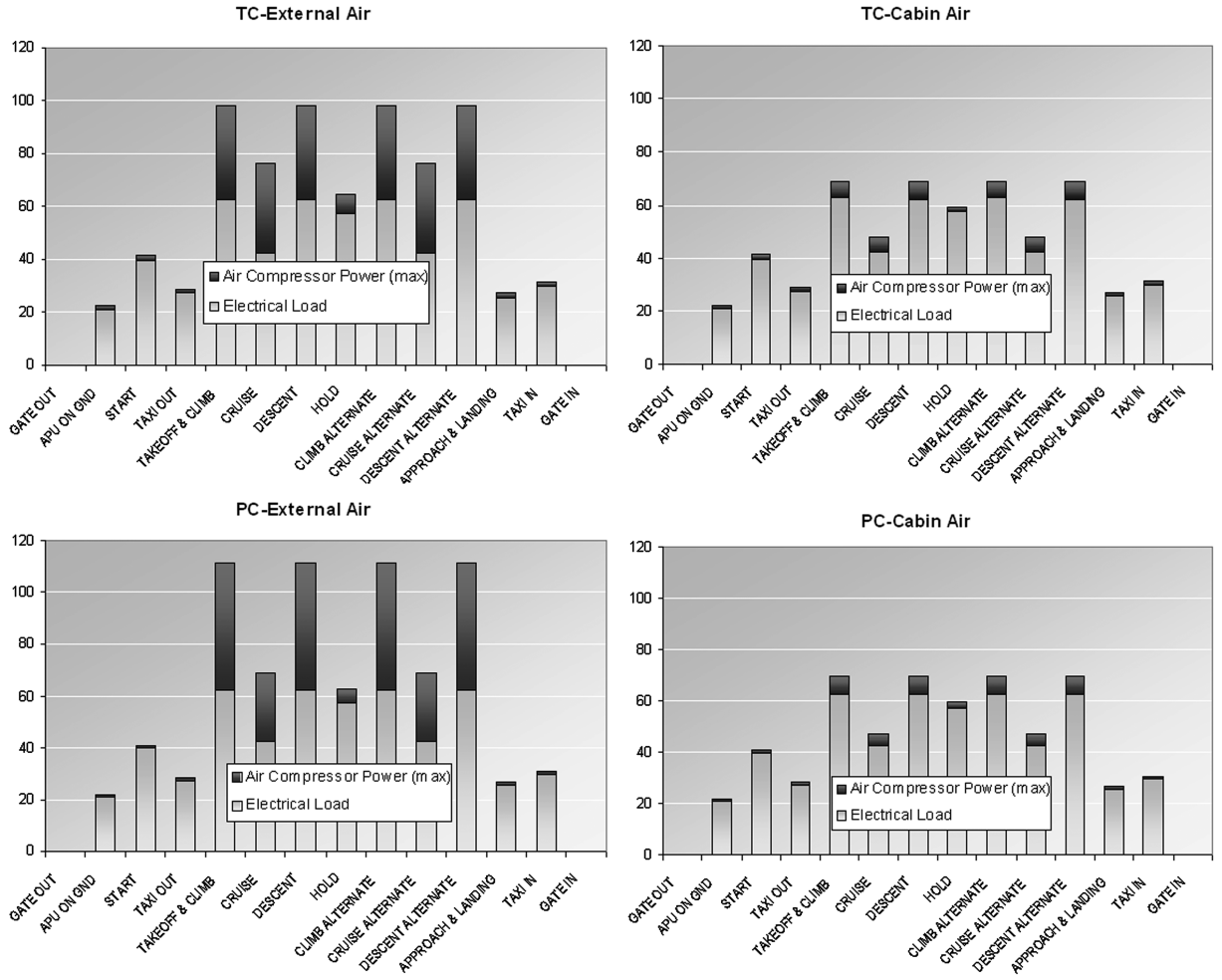

Fig. 8 Impact of the air compression power over the nominal power of the RJ stack (kW).

stack have been estimated, taking into account the geometry and density of each single-cell layer and the number of cells per stack. The thickness and composition of the anode, cathode, electrolyte, and interconnect, as well as the geometrical characteristics of each cell, have been found from literature and direct measurements (SEM analysis) [17]. Planar cells are much more compact and lighter than tubular cells.

The behavior of the current density for the three types of aircraft during the mission is presented in Fig. 7. It can be observed how the PC stack works at higher current densities within a wider regulation range. In fact, for covering the peaks, it could even exceed 900 mA/cm^2, which occurs during the takeoff and climb phase of the regional jet.

Also true for the regional jet, for both geometrical configurations at low loads and low altitude, the stack in case 2 (cabin air), which has fewer cells, will work at higher current densities to produce the same electric power. At high altitudes, even if the TC stack is larger in case 1 (allowing, in principle, reduced current density values compared with case 2 operation), the stack is forced to produce more power to supply the air compressor, and so the current density of operation exceeds that of case 2. Conversely, in the PC, case 2 allows a reduced installed power, causing an increase in the operating current density requested to the stack compared with case 1, in which the stack size is higher.

The behavior of the current density for both geometrical configurations in the air taxi is similar to that of the regional jet: peaks are reached during the climb and descent phases, and the load is reduced during the cruise phase. The main difference is that the highest peak for the air taxi represents the engine start phase, in which the load is more than twice the load of the climb phase. In fact, the size of the stack in this aircraft has been estimated by considering the power for starting up the engine, and it could be halved if another solution were considered for starting up the main engine.

The peaks observed for the air taxi and the regional jet during climbing and descending are not observed in the case of the small commuter; on the contrary, during these phases of the mission, the current density drops in both TC and PC. This is due to the fact that, in these stages of the flight, the heating system is turned off. As previously explained, in this typology of aircraft, the supply of the heating system with an integration between the electric power surplus of the stack and the thermal power recovered from its exhausts has been considered. The power surplus is not necessary when the heating system does not operate, and so the total load decreases, lowering the current demand. As in the case of the air taxi, the maximum peak of the small commuter's mission is reached during the main engine start up and, also in this case, the size of the stack could be reduced if not for this phase. The peak power difference for this aircraft is, however, not as noticeable as it is for the air taxi.

For the regional jet in case 2, in some phases of the mission (in particular, during the cruise phase) in which the gross electric power of the generator is lower due to less work spend on air compression, the recoverable thermal power from the exhaust gases from the stack is not enough for covering the ACH thermal load (see Fig. 10). Thus,

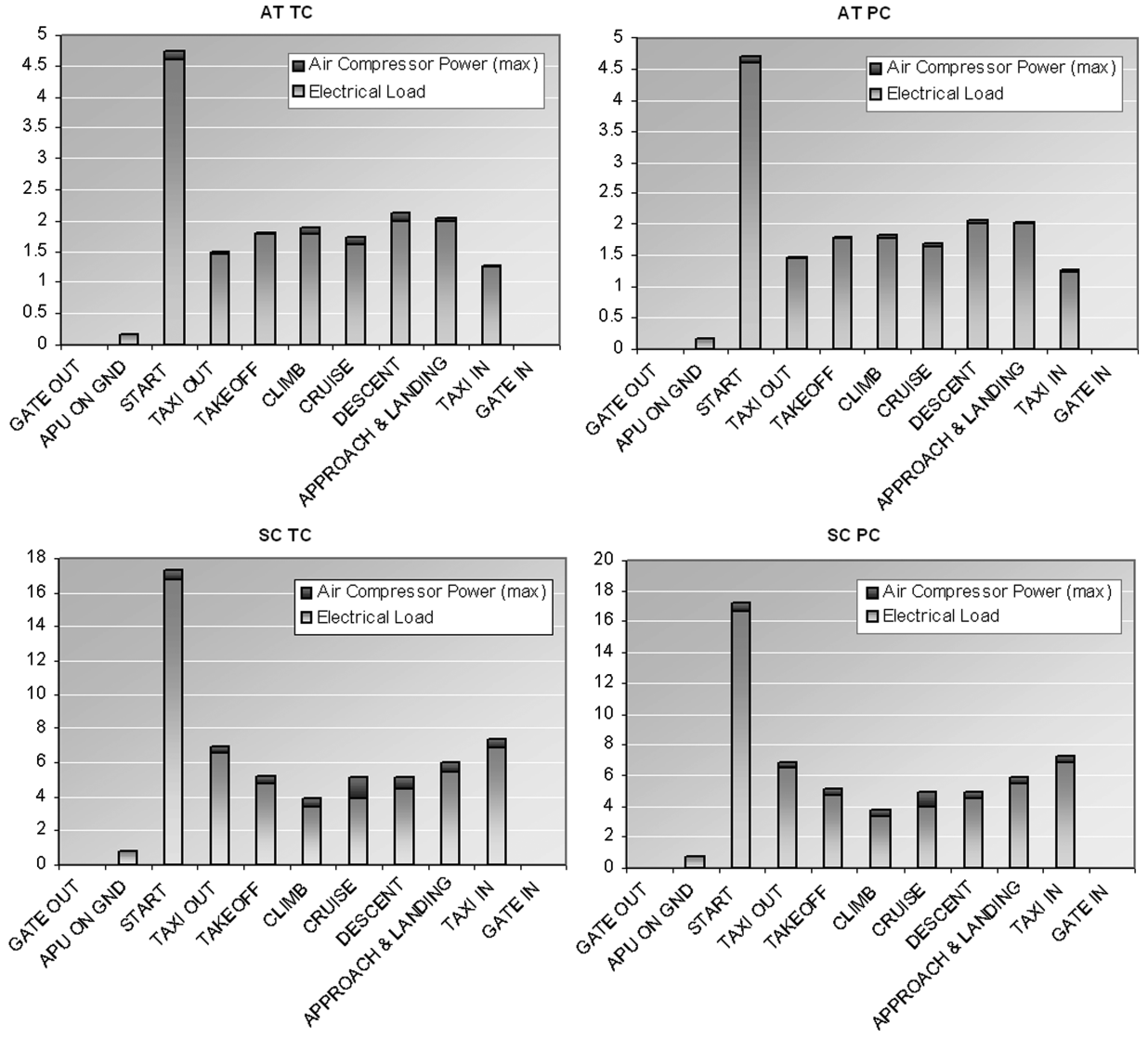

Fig. 9 Impact of the air compression over the nominal power of the AT and SC stack (kW).

it becomes necessary to generate an electric power surplus by increasing the operating current density (as shown in Fig. 7).

The effect that the power consumption of the air compressor has over the gross electric power to be generated by the stack and, therefore, over its nominal power output, can be observed in Fig. 8 (RJ) and Fig. 9 (AT and SC). Because the SOFC generator must supply not only the onboard loads but also the electric power for the compression of feed air, the size of the stack (presented in Table 8) is estimated on the basis of the total electric power output, taking into account, other than the electrical load of the onboard systems, the maximum power request of the air compressor in each phase of the mission.

The effect of air compression on the stack power output is especially marked in the case of the regional jet (see Fig. 8), due to its high-altitude cruise phase (about 30,000 ft) and the low pressure of feed air at the intake of the air compressor, not only when using external air but also in case 2, because the cabin is not kept at atmospheric pressure but it is fixed a pressure differential between the cabin and the external air. It is, however, evident that the use of external air at high altitudes significantly increases the nominal power of the stack and, consequently, also the system mass and volume. And so, from this point of view, the use of cabin air is advantageous.

With regard to the small commuter and the air taxi, as can be observed in Fig. 9, because of the lower altitudes reached during the mission, the power consumption of the air compressor and its effect over the nominal power of the stack is diminished with respect to the regional jet. Particularly in the AT, the maximum power consumption of the air compressor is obtained during the start phase, when the aircraft is on the ground, and it does not significantly affect the size of the stack.

It can be seen how, for both aircraft, the power consumption for the compression of feed air is higher for the TC stack even if the temperature of operation is higher (and so, in principle, requiring more cooling air). This is explained by the lower rates of stoichiometric air required for feeding the PC stack, which operates at a lower current intensity due to the better performance of planar cells (the lower current intensity is due to the reduced active surface in PC, even if the current density is higher, as shown in Fig. 7).

Effective recoverable thermal power in each mission phase of the regional jet and the small commuter is presented in Fig. 10. For the regional jet, it can be observed how, for both geometrical configurations, in few of the mission phases the gross electric power output of the considered stack is not able to produce enough exhaust for covering the ACH thermal load, requiring an electric power surplus. This means a current density increase, especially in case 2, because the recoverable heat in case 1 is greater due to a greater gross electric power output. The load of the ACH system should then be provided partially by electric power, requiring an electric power surplus.

For the small commuter, on the other hand, the bars in Fig. 10 show how the recoverable heat from the SOFC stack is not enough for covering the load of the heating system without electric integration in any of the mission phases in which it operates; thus, the integration with electric power should be performed in all of them. The thermal load is a discrete value, and it is considered only turned on or turned off in each phase.

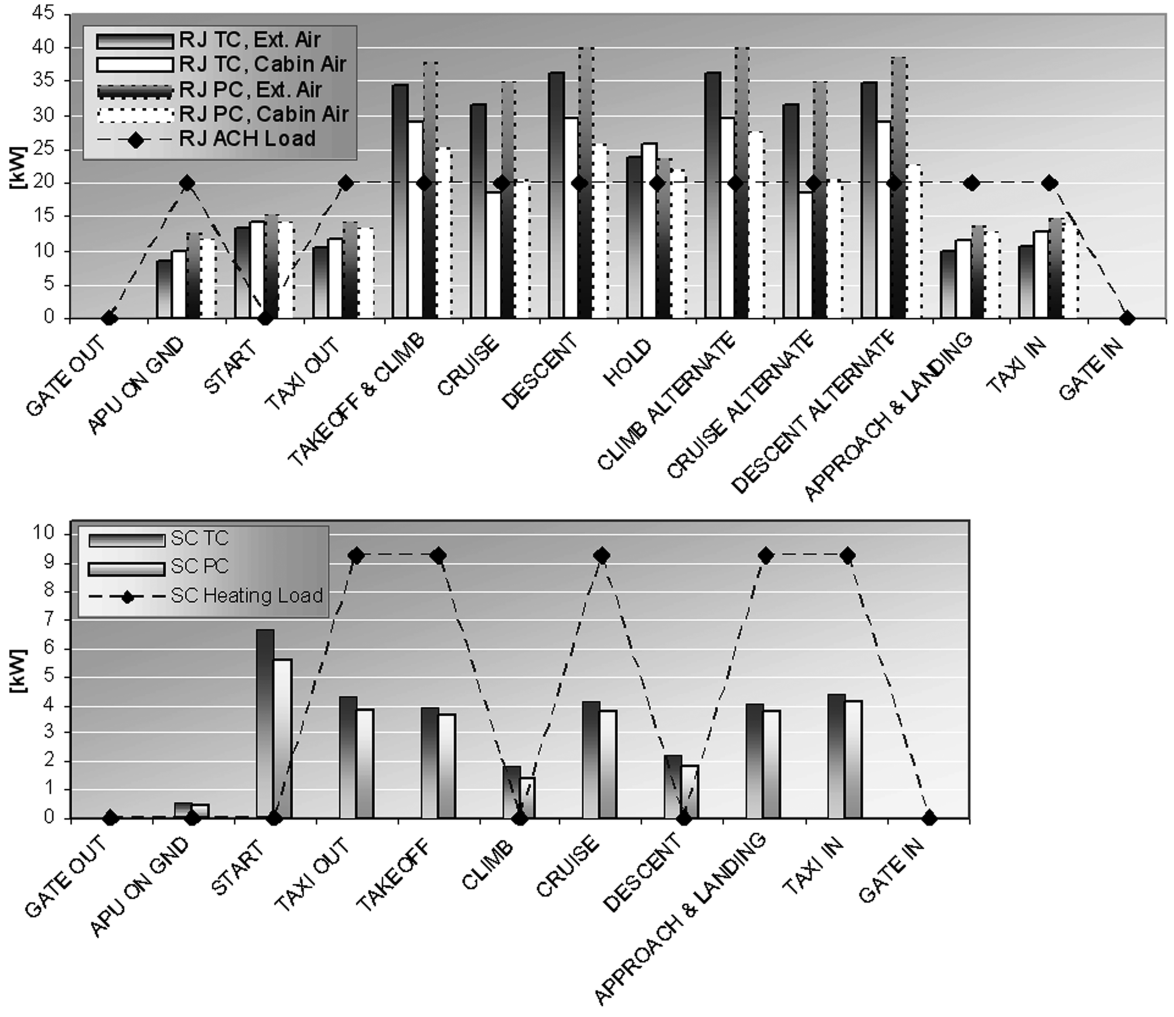

Fig. 10 Effective recoverable thermal power in all mission phases. In the case of the small commuter, the recoverable thermal power alone is not enough to cover the load of the heating system in any of the mission phases.

For both aircraft, in the few phases in which the effective recoverable thermal power is higher than the ACH load, this load is covered and the rest of the energy contained in the exhaust gases is released into the atmosphere, because no other recovery has been hypothesized for any of the analyzed aircraft types. In the phases in which the ACH (RJ) or the heating system (SC) are kept off, all of the energy contained in the exhausts is released into the atmosphere.

Coverage of the ACH load for the regional jet and the heating system for the small commuter in all phases of the mission are described in Fig. 11. The bars in light gray represent the effective thermal power supplied to the ACH or heating system. White bars represent the recoverable thermal power not used and released into the atmosphere. And the darker bars represent the electric power surplus provided to the system during each phase.

Recall that the regional jet's ACH load is equal to 20 kW in all the mission phases except for the startup phase, in which this system is turned off. It can be observed how, during the phases with a low electrical load, less recoverable thermal power is available, so that an

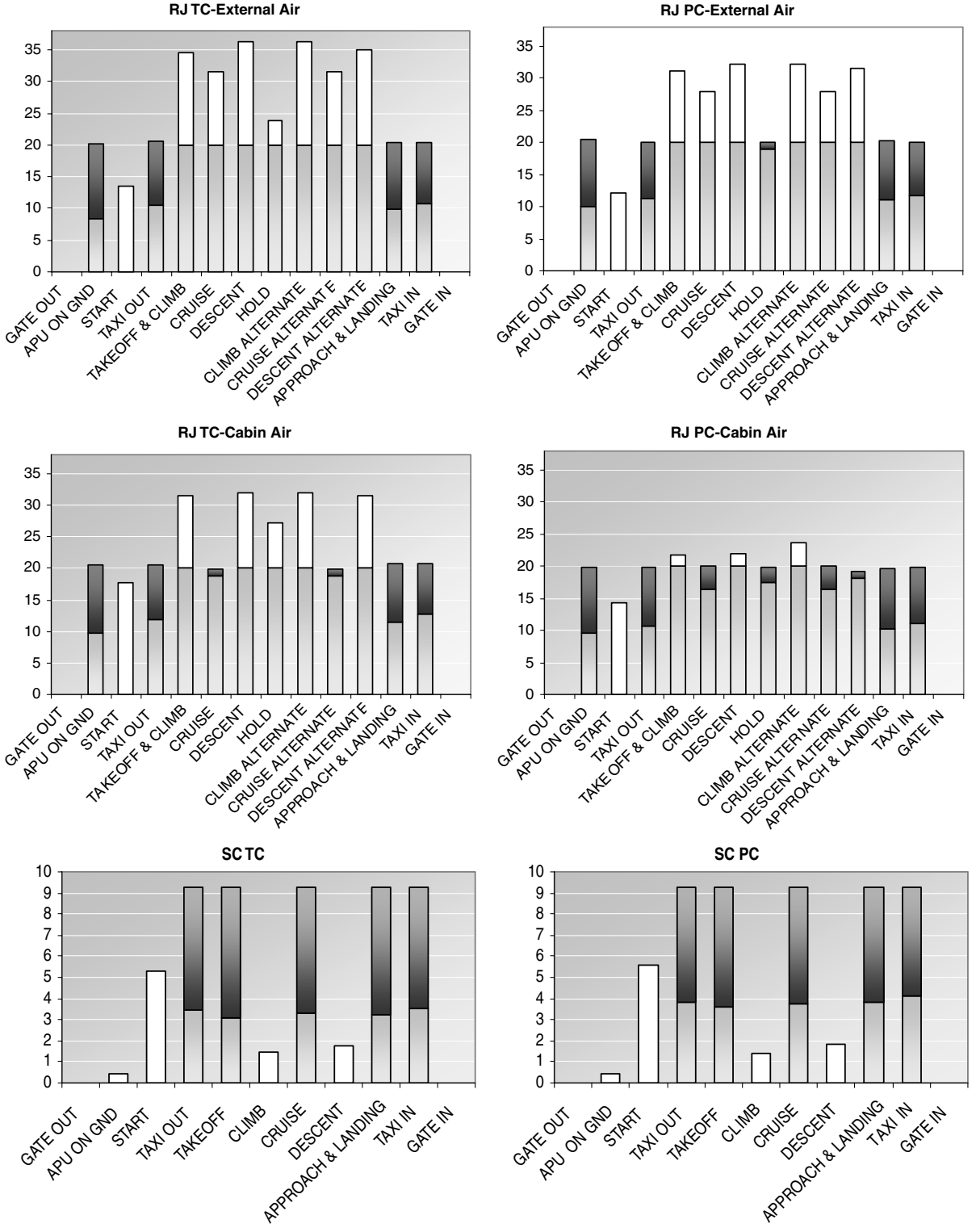

Fig. 11 ACH and heating thermal load coverage in all the mission phases (kW), where the dark bars represent the electric power surplus, the light gray bars represent the used thermal power, and the white bars represent the unused thermal power.

integration with electric power is needed. In case 2, that is, when feeding the SOFC with air from the passenger cabin, less thermal power can be recovered at high altitudes, as already explained, and an electric power surplus is needed for both TC and PC. On the other hand, also in case 2, the unused thermal power lost into the atmosphere is reduced, and so the thermal efficiency of the system is improved.

With a higher electric efficiency and a lower operating temperature in the case of the PC stack, the recoverable heat from the exhaust gas of this stack is lower than that of the TC stack. Hence, in the case of PC, the electric power surplus to be provided to both heating systems in each single mission phase is larger. As an example, in case 1, an electric power surplus is also required for the PC stack during the hold (low altitude) phase, whereas no power surplus is required for the TC stack.

With regard to the small commuter, the load of the heating system is about 9.3 kW only during the phases of taxi out, takeoff, cruise, approach and landing, and taxi in; it is turned off during climb and descent. In all the mentioned phases in which heating operates, electric power should be supplied and, unlike in the regional jet, in the small commuter it does not represent a small fraction of the heating load supplied, but rather it accounts for most of the total power provided to heating. Thus, the all-electric heating system solution for this aircraft could be evaluated, because it would reduce the complexity and the weight added to the system by the heat recovery devices. On the other hand, the fuel consumption of the stack would be augmented and also the mass and volume of the fuel tank.

It is important to note that the darkest bars in Fig. 11 report the electric power surplus for every single phase of the mission;

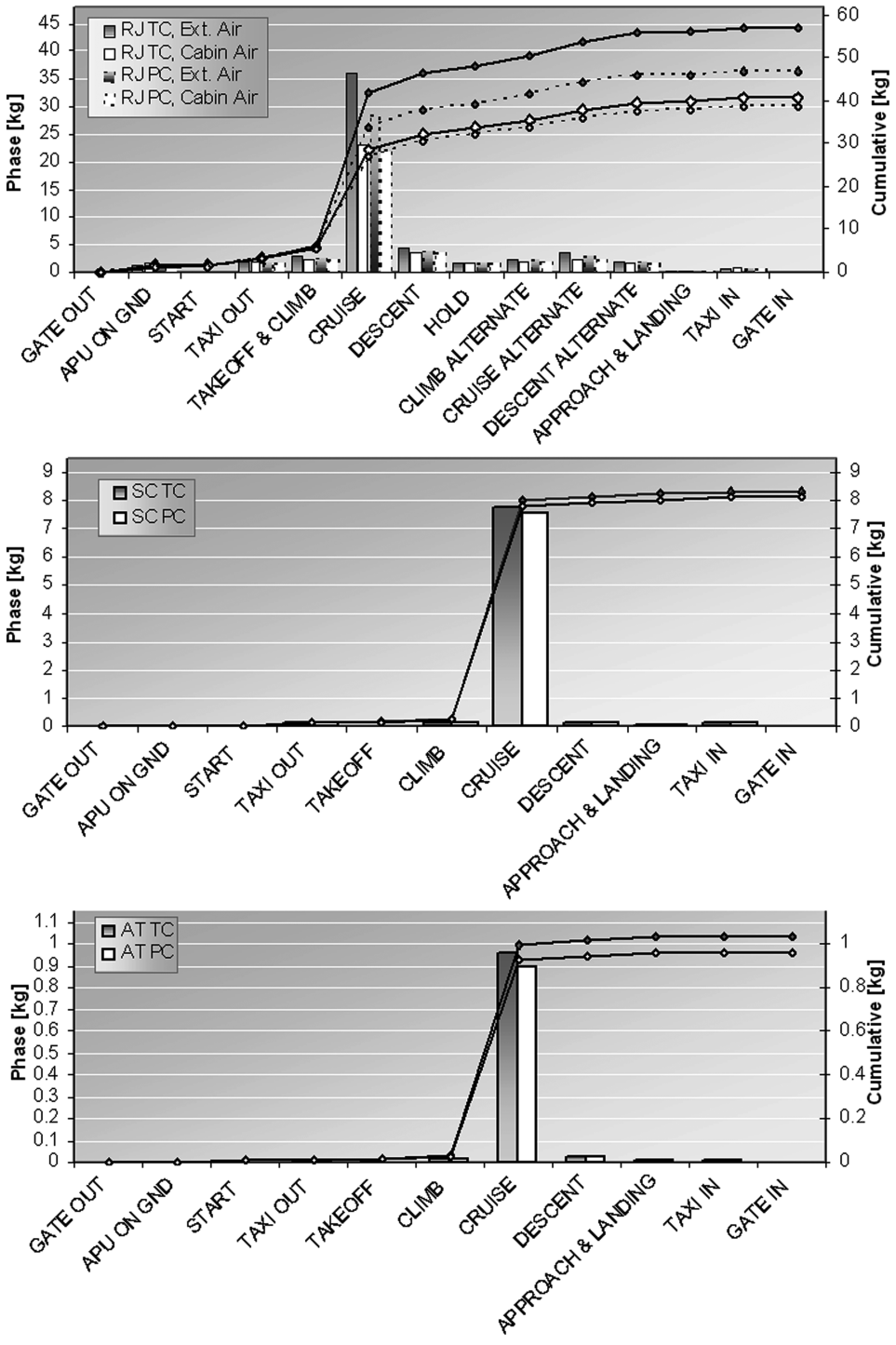

Fig. 12 Fuel consumption in all mission phases and the cumulative consumption.

integrating in time these electric surplus values gives an idea of the energy consumed in terms of kilograms of fuel. In particular, it is observed that the small dark bars in Fig. 11, which indicate low electric power surpluses, could actually represent large extra amounts of consumed fuel, depending on the duration of the mission phase. For example, during cruise, which is the longest phase of the mission (see Fig. 2) for both aircraft, a small electric power surplus represents a considerable increase in fuel consumption.

The fuel consumption in each phase, and the cumulative consumption during the mission, are presented in Fig. 12. For the regional jet, in which four different cases were analyzed, the best option in terms of fuel consumption was the use of cabin air with planar cells, that is, PC case 2, even though this option does not represent the lowest fuel consumption in every single phase of the mission (it is higher than PC case 1 during hold). In fact, PC is advantageous over TC in both of the analyzed system configurations due to better electric performance. In particular, in the case of the PC stack, in which less work is spent on air compression during the cruise phase to the lower stoichiometry (linked to the lower current intensity), the impact of altitude is not as evident as it is for the TC stack, and so the difference in fuel consumption in cases 1 and 2 is significantly reduced.

Also, for the other two types of aircraft (air taxi and small commuter), the fuel consumption when hypothesizing the use of planar cells was lower than that of the TC stack. From the bars in Fig. 12, it can be observed that the duration of the phase is the most significant factor when determining the fuel consumption. In fact, for both aircraft, as the overall load during the start phase is by far the highest, the fuel consumption during this phase is not significant because of the short period in which this load is required. Conversely, even if the overall load is much lower and, consequently, the fuel consumption in terms of grams of natural gas per second is also lower, almost all the fuel spent along the entire mission is consumed during the cruise phase.

To supply the onboard loads during the mission, the conventional systems of the regional jet would consume about 83 kg of fuel [23]. With regard to the air taxi and small commuter, the electrical power is currently provided with batteries. Whereas a 20 kg battery is installed in the air taxi, a 50 kg battery pack is used used in the small commuter [24].

It must be said that the larger surplus of electric power needed by the PC, in the case of the small commuter and the regional jet, causes higher fuel consumption rates. Therefore, if ACH and heating loads were not considered, or a solution different from an electric power integration were hypothesized, the fuel consumption of the PC stack would be even lower and the gap between TC and PC would be augmented in these two typologies as it is for the air taxi (see Fig. 12).

A comparison of the fuel consumption of the regional jet when supplying only electric power to the heating system (original more-electric configuration) and the CHP configuration is presented in Fig. 13. The advantage of recovering heat from the exhaust, otherwise released into the atmosphere, can be seen in terms of fuel consumption. Decreasing the fuel consumption decreases pollutant emissions into the atmosphere.

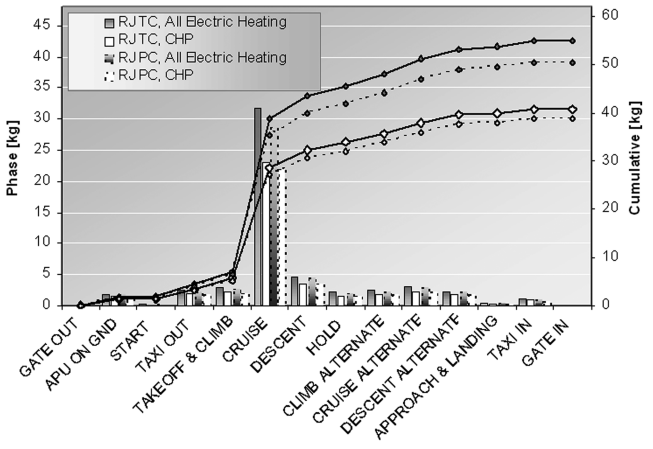

Fig. 13 Fuel consumption for all-electric heating and CHP (RJ cabin air).

VI. Conclusions

The use of fuel cells in aeronautics and, in particular, in passenger planes, is still in the very early phases of development. The ENFICA-FC project, other than being directed to fulfilling a manned flight for a small two-seat aircraft, is focused on studying the feasibility of using fuel-cell systems such as APU as a power supply for the onboard systems of different passenger aircraft as the air taxi, the small commuter, and the regional jet considered in this work.

Many aspects should still be analyzed, and improvements in the fuel cells and fuel storage systems would need to be made before this technology could be able to compete with traditional and long-proven technologies (because the security and reliability of every component is a major issue when it comes to aeronautics). Some conditions characteristic of aeronautical applications, long-employed in stationary power production and automotive applications, are new in the field of fuel cells. For instance, the impact of altitude changes, high inertial forces, the applicability of CHP and hybrid systems, and the use of lighter materials are subjects of continuous research.

Nevertheless, from simulations such as those performed in this work, it is believed that, in a middle-term scenario, a system based on existing fuel-cell technologies could be integrated to small- or midsize aircraft as a power source for the onboard loads during entire missions.

Depending on the type and magnitude of the onboard loads, the use of SOFC-based systems in certain typologies of aircraft could be advantageous over other FC systems such as PEMFC, due to their useful high-temperature exhaust gas, which makes it possible to supply some thermal loads directly with recovered heat; thus, the nominal electric power is reduced and, therefore, the size and mass of the fuel-cell-based electrical system of future more-electric aircraft.

Even when no heat recovery is hypothesized, as in the case of the air taxi, the choice of employing a SOFC system could be beneficial due to the fuel flexibility of this technology. In fact, the ability of SOFCs to use hydrocarbons and high energy-density fuels, including jet fuel, represents a big advantage because no significant modifications would need to be made to current fuel storage and distribution systems and there would be no need for large, heavy, and complex hydrogen storage tanks to be incorporated into the aircraft.

With regard to the geometrical configuration of the cells, which is not dependent on the size of the system or, therefore, on the typology of aircraft in which the system would be placed, the performance of planar SOFCs is better than that of tubular SOFCs due essentially to lower ohmic overpotential. This means lower consumption of fuel when using PC. In addition, planar cells operate at higher current densities, lowering the number of cells required and, with it, the size (mass and volume) of the stack. Concerning the mass and volume, planar cells are much more compact and lighter than tubular cells. Together with their better performance, this geometrical configuration of SOFCs is more likely to be used in mobile applications.

SOFC systems are still heavier than conventional APUs. Nevertheless, scientific research focused on new materials and cell geometries will considerably reduce the mass of the stack and of the BOP, by using lighter components and increasing the power density due to better polarization. Moreover, this weight disadvantage can be offset by fuel savings thanks to the higher SOFC system efficiencies against the main engine bleed and extraction during the cruise phase.

A critical aspect regarding the use of fuel-cell systems in aeronautics is the feed air. It has to be compressed to the pressure of operation of the cell, and the external air is highly affected by altitude changes during the mission, especially in large transport aircraft with high-altitude cruise phases such as the regional jet treated in this work. For this aircraft typology, it has been studied with positive results the possibility of feeding the SOFC stack with pressurized air from the passengers cabin with no major effects on its performance,

lowering the compressor requests and, thus, the nominal power output and the mass of the FC system as well as its consumption of fuel.

Another limiting aspect of SOFCs is long startup times. In this sense, research is focused on lowering the operation temperature of the stack. On the other hand, a SOFC-based APU can be started on the ground a sufficient time before takeoff, in an open circuit sustained with an NH mix flow (5% H_2 in N_2), and kept in standby for days if the aircraft is kept on the ground. From this point of view, among the two SOFC configurations considered in this work, PC could be advantageous because its temperature of operation is lower than that of TC.

Acknowledgments

The authors acknowledge support from the European Commission through the ENFICA-FC project, European Commission Sixth Framework Programme contract no. AST5-CT-2006-030779. The authors would also like to thank all ENFICA-FC partners.

References

[1] International Industry Working Group, *Commercial Aircraft Design Characteristics—Trends and Growth Projections*, 5th ed., International Air Transport Association, Montreal, Jan. 2007.

[2] Warshay, M., and Prokopius, P., "The Fuel Cell in Space: Yesterday, Today and Tomorrow," *Journal of Power Sources*, Vol. 29, Nos. 1–2, Jan. 1990, pp. 193–200. doi:10.1016/0378-7753(90)80019-A

[3] Lapeña-Rey, N., Mosquera, J., Bataller, E., Ortí, F., Dudfield, C., and Orsillo, A., "Environmentally Friendly Power Sources for Aerospace Applications," *Journal of Power Sources*, Vol. 181, No. 2, July 2008, pp. 353–362. doi:10.1016/j.jpowsour.2007.11.045

[4] LaBreche, T., "Solid Oxide Fuel Cell Power Systems for Small UAVs," *2007 Joint Service Power Expo*, April 2007.

[5] Steffen, C. J., Jr., Freeh, J. E., and Larosiliere, L. M., "Solid Oxide Fuel Cell/Gas Turbine Hybrid Cycle Technology For Auxiliary Aerospace Power," NASA TM-2005-213586, 2005.

[6] Mak, A., and Meier, J., *Fuel Cell Auxiliary Power Study Vol. 1: RASER Task Order 5*, Honeywell Engines, Systems & Services, Phoenix, Arizona, Feb. 2007.

[7] Tornabene, R., Wang, X.-Y., Steffen, C. J., Jr., and Freeh, J., "Development of Parametric Mass and Volume Models for an Aerospace SOFC/GAS Turbine Hybrid System," NASA TM-2005-213819, 2005.

[8] Daggett, D., "Product Development, Boeing Fuel Cell APU Overview," *Solid State Energy Conversion Alliance Annual Meeting*, April 2003.

[9] Kohout, L., "Systems Analysis Developed for All-Electric Aircraft Propulsion," *Research & Technology 2003*, Diane Publishing, Darby, PA, 2004, pp. 54–55.

[10] Namazian M. Venkataraman, G., Sethuraman, S., Lux, K., Elder, E., Shalaby, C., Ma, X., and Song, C., "Integrated Distillate-Fuel Desulfurizer and Reformer for SOFC and High Temperature PEM," *Fuel Cell Seminar and Exposition Abstracts for Oral Presentations*, Oct. 2007, pp. 310–313.

[11] Himansu, A., Freeh, J. E., Steffen, C. J., Jr., Tornabene, R., Wang, X.-Y., "Hybrid Solid Oxide Fuel Cell/Gas Turbine System Design for High Altitude Long Endurance Aerospace Missions," NASA TM-2006-214328, 2006.

[12] Shavit, Z., Steses, A., Szachter, A., Aharon, E., Elias, T., Ashkenazi, M., Weintraub, S., Feldman, Y., Frulla, G., Moraglio, I., Cestino, E., Borelo, F., Novarese, C., and Biganovsky, J., "Identification and Requirements of Relevant Electrical Systems for Various Regional Jet Aircraft," IAI-Politecnico di Torino, ENFICA-FC Rept. D2/2, 2007.

[13] Santarelli, M., Leone, P., Calì M., and Orsello, G., "Experimental Analysis of the Voltage and Temperature Behavior of a SOFC Generator," *Journal of Fuel Cell Science and Technology*, Vol. 4, No. 2, May 2007, pp. 143–153. doi:10.1115/1.2713772

[14] Calì M., Santarelli, M., and Leone, P., "Computer Experimental Analysis of the CHP Performance of a 100 kWe SOFC Field Unit by a Factorial Design," *Journal of Power Sources*, Vol. 156, No. 2, June 2006, pp. 400–413. doi:10.1016/j.jpowsour.2005.06.033

[15] Calì M., Santarelli, M., and Leone, P., "Design of Experiments for Fitting Regression Models on the Tubular SOFC CHP 100 kwe: Screening Test, Response Surface Analysis and Optimization," *International Journal of Hydrogen Energy*, Vol. 32, No. 3, March 2007, pp. 343–358. doi:10.1016/j.ijhydene.2006.05.021

[16] Leone P.,Lanzini, A., Squillari, P., Asinari, P., Santarelli, M., Borchiellini, R., and Calì M., "Experimental Evaluation of the Operating Temperature Impact on Solid Oxide Anode Supported Fuel Cells," *International Journal of Hydrogen Energy*, Vol. 33, No. 12, June 2008, doi:10.1016/j.ijhydene.2008.03.042.

[17] Leone, P., "Experiments with Solid Oxide Fuel Cells in Laboratory and Industrial Environments," Ph.D. Thesis, Politecnico di Torino, 2008.

[18] Santarelli, M., Cabrera, M., and Calì M., "SOFC-based APU for Regional Jets: Design and Mission Simulation with Different Cell Geometries," *Journal of Fuel Cell Science and Technology*, (to be published).

[19] Asinari, P., Calì Quaglia, M., Von Spakovsky, M. R., Kasula, B. V., "Direct Numerical Calculation of the Kinematic Tortuosity of Reactive Mixture Flow in the Anode Layer of Solid Oxide Fuel Cells by the Lattice Boltzmann Method," *Journal of Power Sources*, Vol. 170, No. 2, July 2007, pp. 359–375. doi:10.1016/j.jpowsour.2007.03.074

[20] Chen, X. J., Chan, S. H., and Khor, K. A., "Simulation of a Composite Cathode in Solid Oxide Fuel Cells," *Electrochimica Acta*, Vol. 49, No. 11, April 2004, pp. 1851–1861. doi:10.1016/j.electacta.2003.12.015

[21] Zhao, F., and Virkar, A. V., "Dependence of Polarization in Anode-Supported Solid Oxide Fuel Cells on Various Cell Parameters," *Journal of Power Sources*, Vol. 141, No. 1, Feb. 2005, pp. 79–95. doi:10.1016/j.jpowsour.2004.08.057

[22] Prausnitz, J. M., and Poling, B., *The Properties of Gases & Liquids*, 4th ed., McGraw–Hill, New York, 1987.

[23] Shavit, Z., and Romeo, G., "Parametric Sizing of a More-Electric Regional Jet Aircraft," IAI-Politecnico di Torino, ENFICA-FC Rept. D2/5, 2007.

[24] Biganovský J., Navrátil, J., Mikulka, Z., Shavit, Z., and Romeo, G., "Parametric Sizing/Analysis of Vehicle Performance and Characteristics," Evektor—IAI-Politecnico di Torino, ENFICA-FC Rept. D2/4, 2007.